CO_2-driven diffusiophoresis and water cleaning: similarity solutions for predicting the exclusion zone in a channel flow

Suin Shim[1,*], Mrudhula Baskaran[2], Ethan H. Thai[3], and Howard A. Stone[1,†]

[1] *Department of Mechanical and Aerospace Engineering, Princeton University, Princeton, NJ 08544, USA*

[2] *Unsteady Flow Diagnostics Laboratory, Institute of Mechanical Engineering, École Polytechnique Fédérale de Lausanne, 1015, Lausanne, Switzerland*

[3] *Department of Electrical Engineering, Princeton University, Princeton, NJ 08544, USA*

(Dated: July 7. 2021)

In the Supplementary Information, we include additional experiments, details of the theoretical model, and numerical calculations.

1. Long time behavior of the exclusion zone

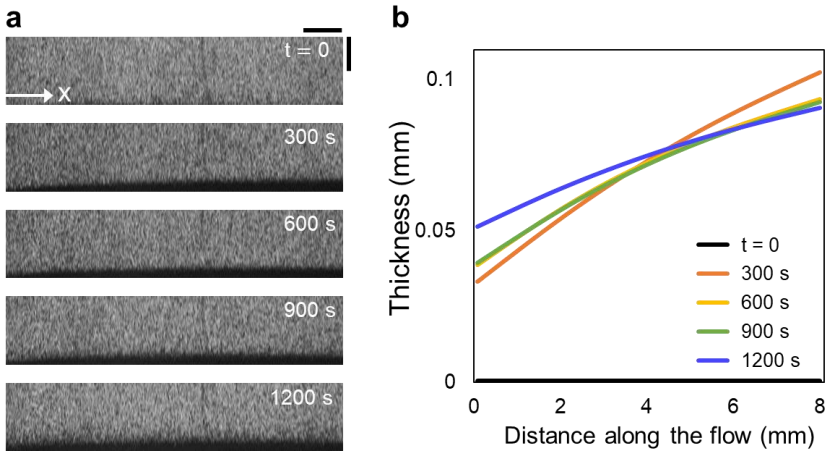

Figure S1: Time evolution of the exclusion zone up to 20 minutes. (a) Time sequence images showing exclusion zone formation in the channel with $w = 1$ mm and $h = 100$ μm at mean flow speed $\langle u \rangle = 100$ μm/s. The horizontal and vertical scale bars are, respectively, 1 mm and 250 μm. (b) The boundary of the exclusion zone plotted versus distance along the flow for different times. Due to the CO_2 diffusion in PDMS, the exclusion of particles occurs from further upstrean, and the thickness of the exclusion zone at $x = 0$ increases over time. The plotted data is obtained from one experiment, and smoothing spline fit is applied.

In the main text (Figure 1(e)) we present the analyses of experimental results up to 10 minutes. We observe that the steady-state exclusion zone lasts longer and we plot the boundary of the exclusion zone in Figure S1(b) up to 20 minutes. As mentioned in the main text, CO_2 diffuses into the PDMS walls in the channel, and makes the exclusion zone form from further upstream over time. As a result, we observe an increase in the exclusion zone at $x = 0$. At larger x, the size of the steady-state exclusion zone remains roughly constant over time. Since the channel is made with PDMS, CO_2 diffusion in PDMS can be one reason for slight decrease in the exclusion zone over long time.

* sshim@princeton.edu
† hastone@princeton.edu

2. Solutions to equation (19)

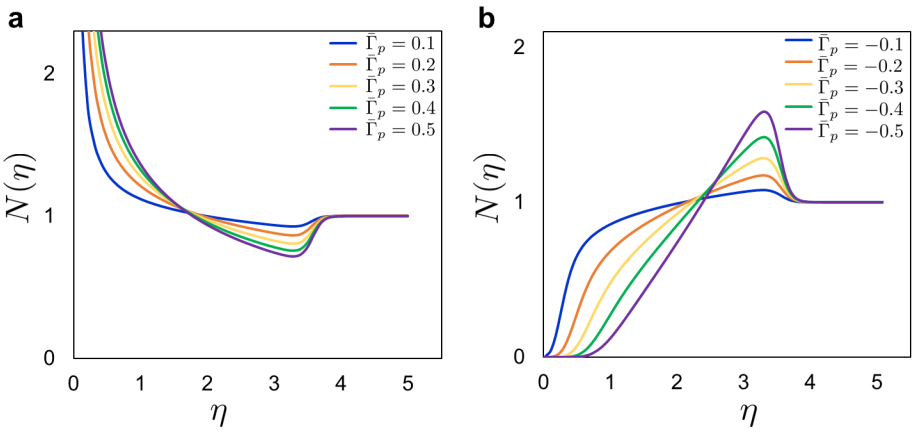

Figure S2: Solutions of equation (19) in the main text are plotted for different values of $\bar{\Gamma}_p$. (a) Positively charged particles ($\bar{\Gamma}_p > 0$) tend to accumulate more as the mobility increases near $\eta \to 0$. (b) Negatively charged particles ($\bar{\Gamma}_p < 0$) move away from the boundary ($\eta = 0$), and the larger the mobility, the more particles are cleared away from the CO_2 boundary.

In the main text, we neglected the particle diffusion term in the equation (20) given the physical condition $D_p \ll |\Gamma_p|$. Here we include the solutions to equation (19) with the particle diffusion considered. Solutions for $\bar{\Gamma}_p = \pm 0.1, \pm 0.2, \pm 0.3, \pm 0.4$ and ± 0.5 are plotted versus η in Figure S2. For the negatively charged particles with the full solutions, the η_c can be defined by setting a threshold concentration for the particle-free region.

3. Flow velocity in a rectangular channel

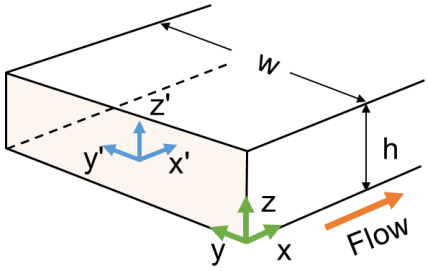

Figure S3: Schematic of a rectangular channel.

In the main text we defined the axes from a corner of the channel. Here we first obtain the flow velocity by defining the axes (x', y', z') from the center of a cross section, and then shift the coordinate to the corner.

The velocity profile of a steady, fully developed pressure-driven flow $u(y', z')$ can be obtained by solving

$$\frac{dp}{dx'} = \mu \left(\frac{\partial^2 u}{\partial y'^2} + \frac{\partial^2 u}{\partial z'^2} \right) , \tag{1}$$

with the boundary conditions $u(\frac{w}{2}, z') = 0$, $\frac{\partial u}{\partial y'}(0, z') = 0$, $u(y', \frac{h}{2}) = 0$, and $\frac{\partial u}{\partial z'}(y', 0) = 0$. The calculated flow velocity is

$$u(y, z) = -\frac{1}{2\mu} \frac{dp}{dx'} \left\{ \left[\left(\frac{h}{2} \right)^2 - z'^2 \right] - \sum_{n=0}^{\infty} a_n \cos \left(\frac{\lambda_n z'}{h/2} \right) \cosh \left(\frac{\lambda_n y'}{h/2} \right) \right\} , \tag{2}$$

where $a_n = \dfrac{h^2(-1)^n}{\lambda_n^3 \cosh(\lambda_n w/h)}$ and $\lambda_n = \dfrac{2n+1}{2}\pi$ $(n = 0, 1, 2, ...)$.

From the volumetric flow rate

$$Q = 4\int_0^{\frac{h}{2}}\int_0^{\frac{w}{2}} u(y',z')dy'dz' = -\frac{wh^3}{12\mu}\frac{dp}{dx}\left[1 - 6\left(\frac{h}{w}\right)\sum_{n=0}^{\infty}\lambda^{-5}\tanh\left(\lambda_n\frac{w}{h}\right)\right] , \tag{3}$$

we obtain the pressure gradient as

$$\frac{dp}{dx} = -\frac{12\mu Q}{wh^3}\left[1 - 6\left(\frac{h}{w}\right)\sum_{n=0}^{\infty}\lambda_n^{-5}\tanh\left(\lambda_n\frac{w}{h}\right)\right]^{-1} . \tag{4}$$

Since the mean flow velocity is defined as $\langle u\rangle = Q/wh$, we can write the velocity (2) in terms of $\langle u\rangle$

$$u(y',z') = \frac{6\langle u\rangle}{h^2}\left[1 - 6\left(\frac{h}{w}\right)\sum_{n=0}^{\infty}\lambda_n^{-5}\tanh\left(\lambda\frac{w}{h}\right)\right]^{-1}\left\{\left[\left(\frac{h}{2}\right)^2 - z'^2\right] - \sum_{n=0}^{\infty}a_n\cos\left(\frac{\lambda_n z'}{h/2}\right)\cosh\left(\frac{\lambda_n y'}{h/2}\right)\right\} . \tag{5}$$

In the experiments, we vary $\langle u\rangle$, w or h, so this form is useful. Then for the axes (x, y, z) defined from the corner the velocity profile u is written as

$$u(y,z) = \frac{6\langle u\rangle}{h^2}\left[1 - \left(\frac{6}{\mathcal{W}}\right)\sum_{n=0}^{\infty}\lambda_n^{-5}\tanh\left(\lambda_n\mathcal{W}\right)\right]^{-1}\left[\left(hz - z^2\right) - \sum_{n=0}^{\infty}a_n\cos\left(\frac{\lambda_n\left(z - \frac{h}{2}\right)}{h/2}\right)\cosh\left(\frac{\lambda_n\left(y - \frac{w}{2}\right)}{h/2}\right)\right] , \tag{6}$$

where $\mathcal{W} = w/h$.

The height-averaged velocity $\bar{u}(y)$ is

$$\bar{u}(y) = \frac{1}{h}\int_0^h u\ dz = \langle u\rangle\left[1 - \left(\frac{6}{\mathcal{W}}\right)\sum_{n=0}^{\infty}\lambda_n^{-5}\tanh\left(\lambda_n\mathcal{W}\right)\right]^{-1}\left[1 - \sum_{n=0}^{\infty}\frac{6\cosh\left(\frac{\lambda_n\left(y - \frac{w}{2}\right)}{h/2}\right)}{\lambda_n^4\cosh\left(\lambda_n\mathcal{W}\right)}\right] , \tag{7}$$

and the shear rates at the walls ($y = 0$ and $y = w$) are

$$\dot{\gamma} = \left.\frac{d\bar{u}(y)}{dy}\right|_{y=0,\ y=w} = \pm\frac{12\langle u\rangle}{h}\left[1 - \left(\frac{6}{\mathcal{W}}\right)\sum_{n=0}^{\infty}\lambda_n^{-5}\tanh\left(\lambda_n\mathcal{W}\right)\right]^{-1}\left[\sum_{n=0}^{\infty}\lambda_n^{-3}\tanh\left(\lambda_n\mathcal{W}\right)\right] . \tag{8}$$

4. Shear rate at the top and bottom walls for different $\mathcal{W}$

We calculated the shear rate on the bottom wall to understand the dependence on $\mathcal{W}$. At $y = \frac{w}{2}$ and $z = 0$, the shear rate is calculated to be

$$\left.\frac{\partial u}{\partial z}\right|_{y=\frac{w}{2},\ z=0} = \frac{12\langle u\rangle}{h}\left[1 - \left(\frac{6}{\mathcal{W}}\right)\sum_{n=0}^{\infty}\lambda_n^{-5}\tanh\left(\lambda_n\mathcal{W}\right)\right]^{-1}\left(\frac{1}{2} - \sum_{n=0}^{\infty}\frac{1}{\lambda_n^2\cosh(\lambda_n\mathcal{W})}\right) , \tag{9}$$

and the rescaled shear rate $\left.\frac{h}{\langle u\rangle}\frac{\partial u}{\partial z}\right|_{y=\frac{w}{2},\ z=0}$ is plotted versus $\mathcal{W}$ in Figure S4. We note that the shear rates on the top and bottom walls are also decreasing when the aspect ratio $\mathcal{W}$ is increased.

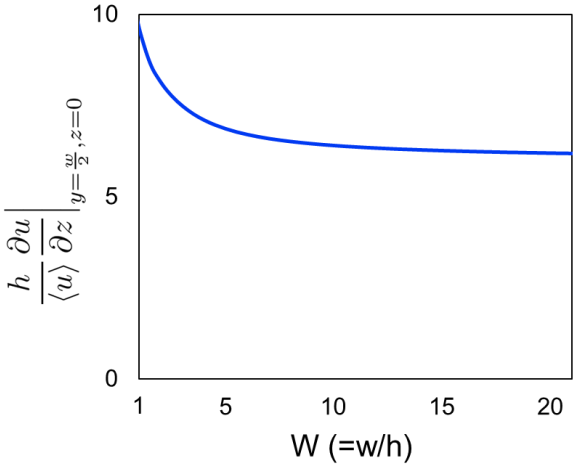

Figure S4: The centerline ($y = w/2$) shear rate on the bottom wall ($z = 0$) of the channel flow.

5. Shear rate ($\dot{\gamma}_z$) calculation

From the velocity profile (equation (6)), we can write the y-averaged flow velocity as

$$\tilde{u}(z) = \frac{1}{w}\int_0^w u\, dy \tag{10}$$

$$= \frac{6\langle u\rangle}{h^2}\left[1 - \left(\frac{6}{\mathcal{W}}\right)\sum_{n=0}^{\infty}\lambda_n^{-5}\tanh\left(\lambda_n\mathcal{W}\right)\right]^{-1}\left[(hz - z^2) - \sum_{n=0}^{\infty}\frac{h^2(-1)^n\tanh(\lambda_n\mathcal{W})}{\mathcal{W}\lambda_n^4}\cos\left(\frac{\lambda_n\left(z-\frac{h}{2}\right)}{h/2}\right)\right]. \tag{11}$$

Then, the two-dimensional shear rate $\dot{\gamma}_z$ for the 90°-rotated orientation is

$$\left.\frac{d\tilde{u}}{dz}\right|_{z=0,z=h} = \pm\frac{6\langle u\rangle}{h}\left[1 - \left(\frac{6}{\mathcal{W}}\right)\sum_{n=0}^{\infty}\lambda_n^{-5}\tanh\left(\lambda_n\mathcal{W}\right)\right]^{-1}\left[1 - \sum_{n=0}^{\infty}\frac{2\tanh(\lambda_n\mathcal{W})}{\mathcal{W}\lambda_n^3}\right]. \tag{12}$$

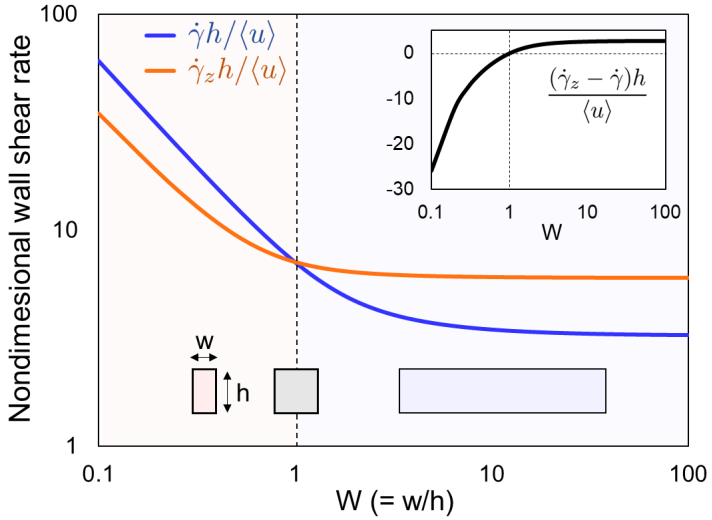

Figure S5: Comparing wall shear rates for two different orientations. Rescaled shear rates ($\dot{\gamma}h/\langle u\rangle$ and $\dot{\gamma}_z h/\langle u\rangle$) are plotted versus $\mathcal{W} = w/h$. For a fixed $\langle u\rangle$ and h, shear rate is always larger when the system is viewed from the narrow-side (i.e. when velocity is averaged through the wide-side). Inset: $(\dot{\gamma}_z - \dot{\gamma})h/\langle u\rangle$ plotted versus $\mathcal{W}$.

6. Three-dimensional advection-diffusion of ions

In the main text we investigate the three-dimensional advection-diffusion of ions to understand possible influence of the z-direction particle velocity on the exclusion zone measurement.

Consider the channel flow described in Section 3, where CO_2 diffuses into the liquid flow through the wall at $y = 0$. We can write advection-reaction-diffusion equations for CO_2 and ion concentrations $c_c(x, y, z, t)$ and $c_i(x, y, z, t)$.[1]

$$\frac{\partial c_c}{\partial t} + u\frac{\partial c_c}{\partial x} = D_c\left(\frac{\partial^2 c_c}{\partial x^2} + \frac{\partial^2 c_c}{\partial y^2} + \frac{\partial^2 c_c}{\partial z^2}\right) - (k_f c_c - k_r c_i^2) \tag{13}$$

$$\frac{\partial c_i}{\partial t} + u\frac{\partial c_i}{\partial x} = D_A\left(\frac{\partial^2 c_i}{\partial x^2} + \frac{\partial^2 c_i}{\partial y^2} + \frac{\partial^2 c_i}{\partial z^2}\right) + (k_f c_c - k_r c_i^2)\ . \tag{14}$$

The initial and boundary conditions are, $c_c(x, y, z, 0) = k_h p_{co_2}$, $c_c(x, 0, z, t) = c_c^{sat}$, $c_c(x, w, z, t) = k_h p_{co_2}$, $\frac{\partial c_c}{\partial z}(x, y, 0, t) = \frac{\partial c_c}{\partial z}(x, y, h, t) = 0$, and $c_c(0, y, z, t) = k_h p_{co_2}$. For ions, $c_i(x, y, z, 0) = \sqrt{k_f k_h p_{co_2}/k_r}$, $\frac{\partial c_i}{\partial y}(x, 0, z, t) = \frac{\partial c_i}{\partial y}(x, w, z, t) = 0$, $\frac{\partial c_i}{\partial z}(x, y, 0, t) = \frac{\partial c_i}{\partial z}(x, y, h, t) = 0$, and $c_i(0, y, z, t) = \sqrt{k_f k_h p_{co_2}/k_r}$. Here, k_h, c_c^{sat}, and p_{co_2} are, respectively, the Henry's law constant of CO_2, saturation concentration of CO_2 in equilibrium with the applied gas pressure at $y = 0$, and the partial pressure of CO_2 in the atmosphere.

The above equations and boundary conditions can be nondimensionalized with $\bar{x} = \frac{x}{h}$, $\bar{y} = \frac{y}{h}$, $\bar{z} = \frac{z}{h}$, $\bar{\bar{u}} = \frac{u}{D_c/h}$, $\tau = \frac{t}{h^2/D_c}$, $Pe = \frac{\langle u\rangle h}{D_c}$, $\bar{c}_c = \frac{c_c}{c_c^{sat}}$, and $\bar{c}_i = \frac{c_i}{\sqrt{k_f k_h p_{co_2}/k_r}}$. Then the nondimensional equations are,

$$\frac{\partial \bar{c}_c}{\partial \tau} + \bar{\bar{u}}\frac{\partial \bar{c}_c}{\partial \bar{x}} = \frac{\partial^2 \bar{c}_c}{\partial \bar{x}^2} + \frac{\partial^2 \bar{c}_c}{\partial \bar{y}^2} + \frac{\partial^2 \bar{c}_c}{\partial \bar{z}^2} - K_1(\bar{c}_c - \bar{c}_i^2) \tag{15}$$

$$\frac{\partial \bar{c}_i}{\partial \tau} + \bar{\bar{u}}\frac{\partial \bar{c}_i}{\partial \bar{x}} = \bar{D}_A\left(\frac{\partial^2 \bar{c}_i}{\partial \bar{x}^2} + \frac{\partial^2 \bar{c}_i}{\partial \bar{y}^2} + \frac{\partial^2 \bar{c}_i}{\partial \bar{z}^2}\right) + K_2(\bar{c}_c - \bar{c}_i^2)\ , \tag{16}$$

where $K_1 = \frac{k_f h^2}{D_c}$ and $K_2 = \frac{k_r h^2\sqrt{k_f k_h p_{co_2}/k_r}}{D_c}$. The nondimensional velocity $\bar{u}$ is

$$\bar{\bar{u}}(\bar{y}, \bar{z}) = 6Pe\left[1 - \left(\frac{6}{\mathcal{W}}\right)\sum_{n=0}^{\infty}\lambda_n^{-5}\tanh(\lambda_n\mathcal{W})\right]^{-1}\left[(\bar{z} - \bar{z}^2) - \sum_{n=0}^{\infty}\frac{(-1)^n}{\lambda_n^3}\cos(\lambda_n(2\bar{z} - 1))\frac{\cosh(\lambda_n(2\bar{y} - \mathcal{W}))}{\cosh(\lambda_n\mathcal{W})}\right]. \tag{17}$$

The nondimensional initial and boundary conditions are, $\bar{c}_c(\bar{x}, \bar{y}, \bar{z}, 0) = \frac{p_{co_2}}{p_c}$, $\bar{c}_c(\bar{x}, 0, \bar{z}, \tau) = 1$, $\bar{c}_c(\bar{x}, \mathcal{W}, \bar{z}, t) = \frac{p_{co_2}}{p_c}$, $\frac{\partial \bar{c}_c}{\partial \bar{z}}(\bar{x}, \bar{y}, 0, \tau) = \frac{\partial \bar{c}_c}{\partial \bar{z}}(\bar{x}, \bar{y}, 1, \tau) = 0$, and $\bar{c}_c(\bar{0}, \bar{y}, \bar{z}, \tau) = \frac{p_{co_2}}{p_c}$, and $\bar{c}_i(\bar{x}, \bar{y}, \bar{z}, 0) = \sqrt{\frac{p_{co_2}}{p_c}}$, $\frac{\partial \bar{c}_i}{\partial \bar{y}}(\bar{x}, 0, \bar{z}, \tau) = \frac{\partial \bar{c}_i}{\partial \bar{y}}(\bar{x}, \mathcal{W}, \bar{z}, \tau) = 0$, $\frac{\partial \bar{c}_i}{\partial \bar{z}}(\bar{x}, \bar{y}, 0, \tau) = \frac{\partial \bar{c}_i}{\partial \bar{z}}(\bar{x}, \bar{y}, 1, \tau) = 0$, and $\bar{c}_i(0, \bar{y}, \bar{z}, \tau) = \sqrt{\frac{p_{co_2}}{p_c}}$.

We solve the coupled partial differential equations numerically with MATLAB, employing an upwinding scheme to avoid numerical instability. The calculation was done in a domain $0 < \bar{x} < 80$, $0 < \bar{y} < \mathcal{W} = 10$ and $0 < \bar{z} < 1$ with a spatial step $\delta x = \delta y = \delta z = 0.1$ and a time step $\delta\tau = 2 \times 10^{-3}$. Solutions to the above equations are presented in Figure 9 in the main text and the effect of the z-direction diffusiophoresis is discussed.

7. Three-dimensional model calculation for the particle exclusion zone

The ion concentration field in the channel flow can be used to calculate the diffusiophoretic velocity of particles. With the boundary layer approximation, the x-direction diffusiophoresis can be neglected. In order to obtain the particle distribution, we can solve

$$\frac{\partial n}{\partial t} + u\frac{\partial n}{\partial x} + \frac{\partial}{\partial y}\left(\Gamma_p\frac{\partial \ln c_i}{\partial y}n\right) + \frac{\partial}{\partial z}\left(\Gamma_p\frac{\partial \ln c_i}{\partial z}n\right) = D_p\left(\frac{\partial^2 n}{\partial x^2} + \frac{\partial^2 n}{\partial y^2} + \frac{\partial^2 n}{\partial z^2}\right)\ , \tag{18}$$

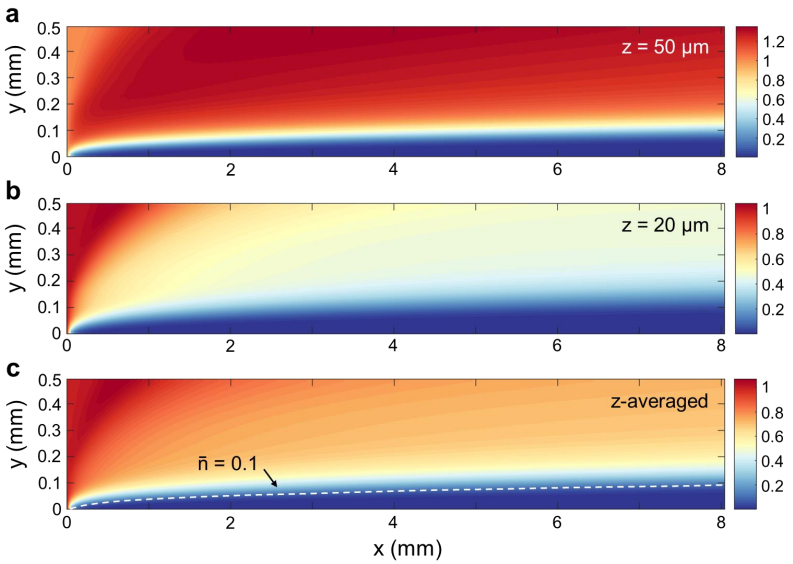

Figure S6: Nondimensional particle concentration $\bar{n}$ plotted versus x and y at (a) $z = 50$ μm and (b) $z = 20$ μm. (c) z-averaged $\bar{n}$ plotted versus x and y. White dashed line is the contour of $\bar{n} = 0.1$.

with boundary conditions

$$n(x, y, z, 0) = n_0 \tag{19a}$$

$$\Gamma_p \frac{\partial \ln c_i}{\partial y} n - D_p \frac{\partial n}{\partial y} = 0 \quad \text{at } y = 0 \quad (\text{for } \Gamma_p < 0\ ; \quad \frac{\partial n}{\partial y} = 0 \text{ for } \Gamma_p > 0) \tag{19b}$$

$$\frac{\partial n}{\partial y} = 0 \quad \text{at} \quad y = w \tag{19c}$$

$$\frac{\partial n}{\partial z} = 0 \quad \text{at} \quad z = 0,\ h \tag{19d}$$

$$n(0, y, z, t) = n_0\ . \tag{19e}$$

Nondimensionalizing the equation and boundary conditions with $\bar{n} = n/n_0$, $\bar{\Gamma}_p = \Gamma_p / D_c$, and $\bar{D}_p = D_p / D_c$, we obtain

$$\frac{\partial \bar{n}}{\partial \tau} + \bar{\bar{u}} \frac{\partial \bar{n}}{\partial \bar{x}} + \frac{\partial}{\partial \bar{y}} \left(\bar{\Gamma}_p \frac{\partial \ln \bar{c}_i}{\partial \bar{y}} \bar{n} \right) + \frac{\partial}{\partial \bar{z}} \left(\bar{\Gamma}_p \frac{\partial \ln \bar{c}_i}{\partial \bar{z}} \bar{n} \right) = \bar{D}_p \left(\frac{\partial^2 \bar{n}}{\partial \bar{x}^2} + \frac{\partial^2 \bar{n}}{\partial \bar{y}^2} + \frac{\partial^2 \bar{n}}{\partial \bar{z}^2} \right)\ , \tag{20}$$

and

$$\bar{n}(\bar{x}, \bar{y}, \bar{z}, 0) = 1 \tag{21a}$$

$$\bar{\Gamma}_p \frac{\partial \ln \bar{c}_i}{\partial \bar{y}} \bar{n} - \bar{D}_p \frac{\partial \bar{n}}{\partial \bar{y}} = 0 \quad \text{at } \bar{y} = 0 \quad (\text{for } \bar{\Gamma}_p < 0\ ; \quad \frac{\partial \bar{n}}{\partial \bar{y}} = 0 \text{ for } \bar{\Gamma}_p > 0) \tag{21b}$$

$$\frac{\partial \bar{n}}{\partial \bar{y}} = 0 \quad \text{at} \quad \bar{y} = \mathcal{W} \tag{21c}$$

$$\frac{\partial \bar{n}}{\partial \bar{z}} = 0 \quad \text{at} \quad \bar{z} = 0,\ 1 \tag{21d}$$

$$\bar{n}(0, \bar{y}, \bar{z}, \tau) = 1\ . \tag{21e}$$

We solve the coupled partial differential equations (12, 13 and 16) numerically with MATLAB, employing an upwinding scheme to avoid numerical instability. Calculations for the CO_2 and ion concentrations were done in a domain $0 < \bar{x} < 80$, $0 < \bar{y} < \mathcal{W} = 10$ and $0 < \bar{z} < 1$ with spatial steps $\delta x = 0.5$, $\delta y = \delta z = 0.1$ and a time step $\delta\tau = 2 \times 10^{-4}$. Particle exclusion is calculated up to $\bar{y} = \mathcal{W}/2$ in the width direction. In Fig. S6 we show the particle distribution at $t = 300$ s for $w = 1$ mm, $h = 100$ μm, $\langle u \rangle = 100$ μm/s (corresponding to $\tau = 60$ and $\mathcal{W} = 10$). Note that the particle distribution varies along the z-direction (Fig. S6(a,b)). We used the height-averaged profile to define an exclusion boundary, where z-averaged $\bar{n} = 0.1$. This exclusion zone boundary is used for comparison with experiments in Fig. 5 of the main text.

8. Effect of diffusioosmosis along the top and bottom walls on the measurement of the exclusion zone

Since the channel walls are charged, we expect that the diffusioosmotic flow is created along the walls by the concentration gradients of CO_2 and ions. We investigate the effect of diffusioosmosis in one extreme regime where there is no pressure-driven flow and the diffusiophoresis of particles is driven by the diffusion of ions. In this case, we can solve for the two-dimensional advection-diffusion (-reaction) of CO_2 and ions in the cross-section of the channel where the advective velocity is induced by the wall diffusioosmosis.

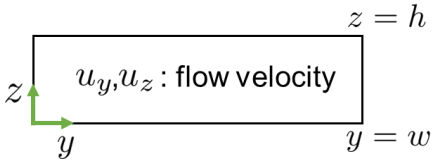

Figure S7: Schematic of the y-z cross section of the channel. The flow velocity u_y and u_z are induced by the diffusioosmosis along the top and bottom walls.

Let u_y and u_z the y- and z-components of the flow velocity induced by wall diffusioosmosis. There is no net flux in this plane (Figure S7) and the velocities follow the continuity equation $\frac{\partial u_y}{\partial y} + \frac{\partial u_z}{\partial z} = 0$. We account for the diffusioosmosis along the top and bottom walls to obtain u_y. Since the height of the channel is smaller than the width, we can use the lubrication approximation for the flow equation.

$$\mu \frac{\partial^2 u_y}{\partial z^2} = \frac{\partial p}{\partial y} \ , \qquad \frac{\partial p}{\partial z} = 0 \ . \tag{22}$$

Let v_s the slip velocity at $z = 0$ and $z = h$ generated by diffusioosmosis, then we obtain u_y as

$$u_y = \frac{1}{2\mu} \frac{\partial p}{\partial y} (z^2 - hz) + v_s \ . \tag{23}$$

Since there is no net flux in the y-z cross section,

$$\int_0^h u_y dz = \frac{1}{6\mu} \frac{\partial p}{\partial y} h^3 - \frac{1}{4\mu} \frac{\partial p}{\partial y} h^3 + v_s h = 0 \ , \tag{24}$$

and

$$\therefore \quad \frac{\partial p}{\partial y} = \frac{12 \mu v_s}{h^2} \ . \tag{25}$$

Let Γ_w be the diffusioosmotic mobility (equivalent to the diffusiophoretic mobility of a particle), then we can write u_y as

$$u_y(y, z) = -\Gamma_w \frac{\partial \ln c_i}{\partial y} \left[6 \left(\frac{z}{h} \right)^2 - 6 \left(\frac{z}{h} \right) + 1 \right] \ . \tag{26}$$

From the continuity equation, we obtain u_z

$$u_z(y, z) = \Gamma_w z \frac{\partial^2 \ln c_i}{\partial y^2} \left[2 \left(\frac{z}{h} \right)^2 - 3 \left(\frac{z}{h} \right) + 1 \right] \ . \tag{27}$$

Now consider the advection-diffusion-reaction equations for CO_2 and ions;

$$\frac{\partial c_c}{\partial t} + u_y \frac{\partial c_c}{\partial y} + u_z \frac{\partial c_c}{\partial z} = D_c \left(\frac{\partial^2 c_c}{\partial y^2} + \frac{\partial^2 c_c}{\partial z^2} \right) - (k_f c_c - k_r c_i^2) \tag{28}$$

$$\frac{\partial c_i}{\partial t} + u_y \frac{\partial c_i}{\partial y} + u_z \frac{\partial c_i}{\partial z} = D_A \left(\frac{\partial^2 c_i}{\partial y^2} + \frac{\partial^2 c_i}{\partial z^2} \right) + (k_f c_c - k_r c_i^2) \ . \tag{29}$$

The equations can be nondimensionalized by

$$\bar{y} = \frac{y}{h} \ , \quad \bar{z} = \frac{z}{h} \ , \quad \tau = \frac{t}{h^2/D_c} \ , \quad \bar{u}_y = \frac{u_y}{D_c/h} \ , \quad \bar{u}_z = \frac{u_z}{D_c/h} \ , \quad \bar{c}_c = \frac{c_c}{c_c^{\rm sat}} \ , \quad \bar{c}_i = \frac{c_i}{c_i^{\rm sat}} \ , \tag{30}$$

and the nondimensional equations are

$$\frac{\partial \bar{c}_c}{\partial \tau} + \bar{u}_y \frac{\partial \bar{c}_c}{\partial \bar{y}} + \bar{u}_z \frac{\partial \bar{c}_c}{\partial \bar{z}} = \frac{\partial^2 \bar{c}_c}{\partial \bar{y}^2} + \frac{\partial^2 \bar{c}_c}{\partial \bar{z}^2} - \frac{\tau_D}{\tau_i} \left(\frac{k_f}{k_r c_c^{\rm sat}} \right)^{\frac{1}{2}} (\bar{c}_c - \bar{c}_i^2) \tag{31}$$

$$\frac{\tau_i}{\tau_D} \left[\frac{\partial \bar{c}_i}{\partial \tau} + \bar{u}_y \frac{\partial \bar{c}_i}{\partial \bar{y}} + \bar{u}_z \frac{\partial \bar{c}_i}{\partial \bar{z}} - \frac{D_A}{D_c} \left(\frac{\partial^2 \bar{c}_i}{\partial \bar{y}^2} + \frac{\partial^2 \bar{c}_i}{\partial \bar{z}^2} \right) \right] = \bar{c}_c - \bar{c}_i^2 \ . \tag{32}$$

$\tau_D = \dfrac{h^2}{D_c}$, $\tau_i = (k_r c_i^{\rm sat})^{-1}$, and $\left(\dfrac{k_f}{k_r c_c^{\rm sat}} \right)^{\frac{1}{2}} = \dfrac{c_i^{\rm sat}}{c_c^{\rm sat}}$. Therefore, for $\tau_i \ll \tau_D$ and $\dfrac{c_i^{\rm sat}}{c_c^{\rm sat}} \ll 1$ we can approximate the above equations as[1]

$$\frac{\partial \bar{c}_c}{\partial \tau} + \bar{u}_y \frac{\partial \bar{c}_c}{\partial y} + \bar{u}_z \frac{\partial \bar{c}_c}{\partial \bar{z}} = \frac{\partial^2 \bar{c}_c}{\partial \bar{y}^2} + \frac{\partial^2 \bar{c}_c}{\partial \bar{z}^2} \quad \text{and} \quad \bar{c}_i = \sqrt{\bar{c}_c} \ . \tag{33}$$

If the channel height is $h = 100$ μm and the applied CO_2 pressure is 10 psi, $\tau_D = 5$ s, $\tau_i = 0.1$ s, $\dfrac{c_i^{\rm sat}}{c_c^{\rm sat}} \approx 0.04$, and thus the approximation is valid.[2–4] The second equation in (25) $\bar{c}_i = \sqrt{\bar{c}_c}$ in dimensional form is $k_f c_c - k_r c_i^2 = 0$ so we call this the local chemical equilibrium approximation. Initial and boundary conditions for $\bar{c}_c$ are, $\bar{c}_c(\bar{y}, \bar{z}, 0) = \frac{p_{\rm co_2}}{p_c}$, $\bar{c}_c(0, \bar{z}, \tau) = 1$, $\bar{c}_c(\mathcal{W}, \bar{z}, \tau) = \frac{p_{\rm co_2}}{p_c}$, and $\frac{\partial \bar{c}_c}{\partial \bar{z}}(\bar{y}, 0, \tau) = \frac{\partial \bar{c}_c}{\partial \bar{z}}(\bar{y}, 1, \tau) = 0$

Next, we solve for the particle distribution in the y-z plane, considering the effect of diffusioosmosis. The advection-diffusion equation for the particle concentration $n(y, z, t)$ is

$$\frac{\partial n}{\partial t} + \frac{\partial}{\partial y} \left[\left(u_y + \Gamma_p \frac{\partial \ln c_i}{\partial y} \right) n \right] + \frac{\partial}{\partial z} \left[\left(u_z + \Gamma_p \frac{\partial \ln c_i}{\partial z} \right) n \right] = D_p \left(\frac{\partial^2 n}{\partial y^2} + \frac{\partial^2 n}{\partial z^2} \right) \ , \tag{34}$$

and the initial and boundary conditions are $n(y, z, 0) = n_0$, $\left(u_y + \Gamma_p \frac{\partial \ln c_i}{\partial y} \right) n \big|_{y=0} - D_p \frac{\partial n}{\partial y} \big|_{y=0} = 0$, $\frac{\partial n}{\partial y} \big|_{y=w} = 0$, and $\frac{\partial n}{\partial z} = 0$ at $z = 0$ and $z = h$.

The nondimensional equation and the boundary conditions are

$$\frac{\partial \bar{n}}{\partial \tau} + \frac{\partial}{\partial \bar{y}} \left[\left(\bar{u}_y + \frac{\bar{\Gamma}_p}{2} \frac{\partial \ln \bar{c}_c}{\partial \bar{y}} \right) \bar{n} \right] + \frac{\partial}{\partial \bar{z}} \left[\left(\bar{u}_z + \frac{\bar{\Gamma}_p}{2} \frac{\partial \ln \bar{c}_c}{\partial \bar{z}} \right) \bar{n} \right] = \bar{D}_p \left(\frac{\partial^2 \bar{n}}{\partial \bar{y}^2} + \frac{\partial^2 \bar{n}}{\partial \bar{z}^2} \right) \ , \tag{35}$$

$\bar{n}(\bar{y}, \bar{z}, 0) = 1$, $(\bar{u}_y + \frac{\bar{\Gamma}_p}{2} \frac{\partial \ln \bar{c}_c}{\partial \bar{y}}) \bar{n} - \bar{D}_p \frac{\partial \bar{n}}{\partial \bar{y}} = 0$ for $\bar{\Gamma}_p < 0$ at $\bar{y} = 0$, and $\frac{\partial \bar{n}}{\partial \bar{y}} \big|_{\bar{y}=\mathcal{W}} = \frac{\partial \bar{n}}{\partial \bar{z}} \, _{\bar{z}=0,h} = 0$. We do not study positively charged particles, but due to the direction of the motion where particles accumulate toward $\bar{y} = 0$, the boundary condition for $\bar{\Gamma}_p > 0$ at $\bar{y} = 0$ is simply $\frac{\partial \bar{n}}{\partial \bar{y}} = 0$.

The nondimensional flow velocities are

$$\bar{u}_y(\bar{y}, \bar{z}) = -\frac{\bar{\Gamma}_w}{2} \frac{\partial \ln \bar{c}_c}{\partial \bar{y}} (6\bar{z}^2 - 6\bar{z} + 1) \tag{36}$$

$$\bar{u}_z(\bar{y}, \bar{z}) = \frac{\bar{\Gamma}_w}{2} \bar{z} \frac{\partial^2 \ln \bar{c}_c}{\partial \bar{y}^2} (2\bar{z}^2 - 3\bar{z} + 1) \ , \tag{37}$$

where $\bar{\Gamma}_w = \Gamma_w / D_c$.

The height-averaged particle distribution is calculated for different aspect ratios of the channels and plotted in Figure 9(i) of the main text. The results show that the effect of diffusioosmosis on the particle distribution is negligible.

9. Multiple CO_2 sources and concentration of ions

In the two-stage system experiment, we included the "break" stage corresponding to a discontinuous region over which CO_2 is supplied at the boundary, in order to reduce the absolute amount of the ions while keeping the direction of the ion concentration gradient the same. In order to visualize this concept, we performed a model calculation using the identical geometry and flow conditions used for Section 6 in the SI (Section 7 in the main text), while introducing CO_2 only for $\bar{x} < 20$ and $\bar{x} > 40$. The numerical calculations were performed up to $\tau = 60$ which corresponds to $t = 300$ s for the channel with $w = 1$ mm and $h = 100$ μm. We plot the ion concentration profiles and $\bar{y}$-component of the diffusiophoretic velocity in Figure S8.

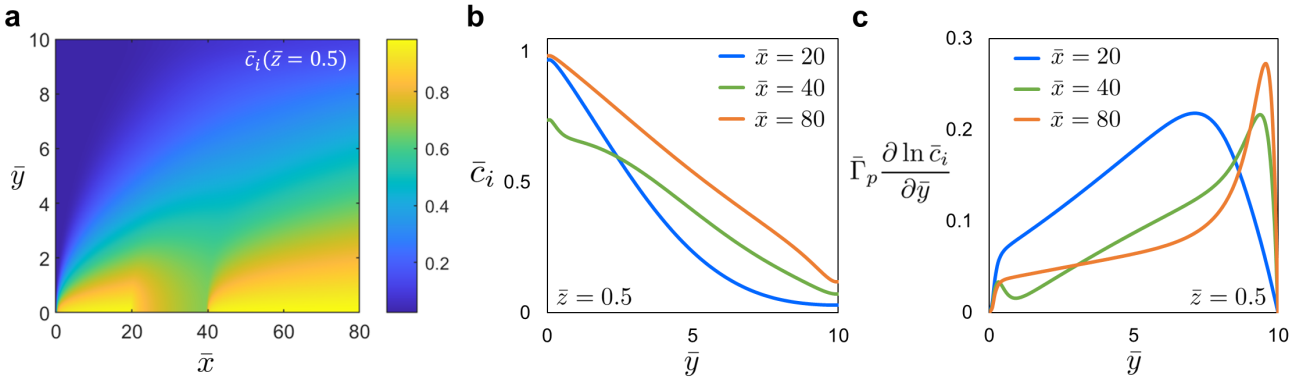

Figure S8: (a) Ion concentration profile plotted versus $\bar{x}$ and $\bar{y}$. Discontinuous CO_2 sources produce uneven concentration profiles along the flow. (b) Comparing the ion concentration at different $\bar{x}$ positions. We note that at $\bar{x} = 40$ (end of the break stage) the absolute concentration of ions is decreased compared to that at $\bar{x} = 20$. (c) $\bar{y}$-component of diffusiophoretic velocity plotted versus $\bar{y}$. In all $\bar{x}$ positions the velocity is positive, showing that the particle motion remains in the same direction in the break stage.

References

[1] S. Shim, S. Khodaparast, C.-Y. Lai, J. Yan, J. T. Ault, B. Rallabandi, O. Shardt, and H. A. Stone, CO_2-driven diffusiophoresis for maintaining a bacteria-free surface. *Soft Matter,* 2021, **17,** 2568-2576.

[2] W. M. Haynes, *CRC Handbook of Chemistry and Physics* (CRC Press, 2015), 96th edn.

[3] C. L. Yaws, *Handbook of Properties for Environmental and Green Engineering*, 1st edn., Gulf Publishing Company (2008)

[4] W. L. Jolly, *Modern Inorganic Chemistry* (McGraw-Hill, New York, 1991), 2nd edn.